Estimation of Rabbit Pancreas Dispersion Between 400 and 1000 nm

Inês Martins[1,2], Hugo Silva[1,2], Valery V. Tuchin[3,4,5], and Luís Oliveira[1,2*]

[1] Physics Department, School of Engineering, Polytechnic Institute of Porto,
Rua Dr. António Bernardino de Almeida 431, 4249-015 Porto, Portugal

[2] Center of Innovation in Engineering and Industrial Technology, ISEP, Rua Dr. António Bernardino de Almeida 431, 4249-015 Porto, Portugal

[3] Science Medical Center, Saratov State University, 83 Astrakhanskaya str.,
Saratov 410012, Russian Federation

[4] Interdisciplinary Laboratory of Biophotonics, National Research Tomsk State University, 36 Lenin's av.,
Tomsk 634050, Russian Federation

[5] Laboratory of Laser Diagnostics of Technical and Living Systems, Precision Mechanics and Control Institute of the Russian Academy of Sciences, 24 Rabochaya str., Saratov 410028, Russian Federation

*** e-mail:** lmo@isep.ipp.pt

Abstract. Current biophotonics methods cover the entire optical spectrum from the deep ultraviolet to the terahertz. To optimize such methods for diagnostic and therapeutic applications, the need to obtain the wideband dispersion of tissues is high. The pancreas is a very important organ in the human body, since it produces insulin and its malfunction may induce diabetes. A reduced number of biophotonics publications regarding the pancreas is available, meaning that studies to determine its optical properties and their variation during optical clearing treatments are necessary. Considering this fact, we used the total internal reflection method to measure the refractive index of the rabbit pancreas for wavelengths between 400 and 850 nm. The experimental results allowed to calculate the pancreas dispersion with the Cauchy, Conrady and Cornu equations. It was observed that all those equations provided good data fitting in the spectral range of the measurements, but differences were observed outside these limits. Considering the wavelength of 633 nm, the mean value from the three dispersions was 1.3521, while the one published for porcine pancreas is 1.3517. The dispersion calculated with the Conrady equation does not present a fast decreasing behavior for shorter wavelengths as the ones calculated with the Cauchy and Cornu equations, but comparing these curves with a dispersion for a tissue-like material, all seem to have good agreement.

Keywords: pancreas tissue; refractive index; total internal reflection; tissue dispersion.

Paper #3409 received 13 Mar 2021; revised manuscript received 8 Apr 2021; accepted for publication 12 Apr 2021; published online 8 May 2021. doi: 10.18287/JBPE21.07.020303.

1 Introduction

Among the various optical properties of biological tissues, the refractive index (RI) is one of the most important and fundamental, since it can be used for many biophotonics applications. If, from one hand, the RI can be a practical measurement to mark pathologies [1–3], it is needed, on the other hand, to estimate the other optical properties through inverse simulations [4], to correct optical coherence tomography (OCT) or microscopy

images [5–7] and to optimize light tissue interactions in diagnostic or treatment procedures [8–10].

Clinical applications of light can be made at various wavelengths within a very wide spectral range that goes from the deep ultraviolet (UV) to the terahertz (THz) [11]. Consequently, the determination of tissue's dispersions for a broad range of wavelengths is of great interest.

The evaluation of tissues' dispersions is also of great interest for the application of optical clearing (OC) treatments, since the exchange of interstitial tissue water by an optical clearing agent (OCA) induces RI variations that will be responsible for the light scattering decrease and consequent increase in tissue transparency [12]. For such particular application, the knowledge of the tissue dispersion and of the dispersions of its components is highly important [13, 14].

While in the THz range, direct RI measurement of biological tissues and OCAs for a wide spectral range is possible [15, 16], in the ultraviolet-near infrared (UV–NIR) range such methodology is not possible, and dispersion calculations must be made from discrete measurements [4, 17–19]. There are some distinct methods to measure the RI of biological samples at discrete wavelengths, such as the ones based on interferometer or ellipsometer setups [20], but the most commonly used nowadays are the ones that use multi-wavelength refractometers [18] or the total internal reflection setup to be used with various lasers at different wavelengths [21]. Other techniques to measure the RI of biological tissues and the importance of these measurements for optical diagnosis have also been recently described [22]. Although the multi-wavelength refractometers provide results with better precision, the setup based on the total internal reflection method can be easily implemented in any optics laboratory at a reduced cost. Another benefit of this method is that additional wavelengths can be selected for measurement, provided that lasers are available at those wavelengths. The total internal reflection was first proposed by Li and Xie in 1996 to measure the RI of biological tissues [21], and it has been widely used since then to measure the RI and estimate the correspondent dispersions for various tissues, such as human normal and pathological colorectal tissues [23, 24], human normal and pathological liver tissues [19, 25], porcine skin [26], or human skin [27]. An improvement to this setup was presented by Deng et al in 2015 [28], which allows a fast determination of the continuous wavelength dependence of the biological materials' RI for a limited spectral range. Such setup, uses a broad-band xenon lamp and a spectrometer to perform measurements [29], making it beneficial for a fast dispersion calculation, but it uses more expensive instrumentation.

Pancreas is an organ that plays an important role in human and animal physiology. It is responsible for the production of insulin that prevents the occurrence of diabetes [30]. Pancreatic cancer, on the other hand, although rare, has presented an increasing number of cases over the years [31]. Due to the lack of early-diagnostic and treatment procedures, the pancreatic cancer is highly lethal. Although some reviews on treatment methods for this pathology have been carried out, the results have been disappointing [32]. Pancreatic ductal adenocarcinoma (PDAC) is the type of cancer with the most lethal malignancies in humans, where a huge percentage of the patients presents an advanced stage and a life expectancy less than 1 year after diagnosis. This problem is largely due to the low number of immunotherapy and drug approaches that target driver mutations [33]. An identification of the risk factors and an early diagnosis are very important to improve overall survival. There are some risk factors that have been reported, like the pancreatic duct dilation, chronic pancreatitis, pancreatic cyst, intraductal papillary mucinous neoplasia (IPMN), and the deterioration of diabetes mellitus [34]. In comparison to other cancers, pancreatic cancer has a wide range of metastatic diseases, like carcinomas at the time of diagnosis, from localized 1–2 cm primary tumors to diffuse carcinomatosis within and outside the abdomen [35].

Regarding biophotonics, pancreas is one of the biological organs that is less studied. From the few optical studies on pancreas, there is one regarding OCT imaging of pancreas with needles for in-depth image acquisition [36], and another that suggests the potential of tissue optical spectroscopy to characterize the human pre-cancerous neoplasms in human pancreatic tissues [37]. A third study has been reported [38], showing the visible spectra for the measured fluorescence and for the estimated absorption and reduced scattering coefficients from human pancreatic tissues (normal, adenocarcinoma and pancreatitis) for comparison.

More recently, two other pancreas-related papers have been published. These papers [39, 40], report on studies about blood microcirculation and blood flow monitoring in rat pancreas with alloxan diabetes by laser speckle contrast imaging, and show that the disease development in animals induces changes in the microcirculatory system response to the application of optical clearing solutions.

The improvement of such techniques or the development of new optical approaches for pancreas imaging or spectroscopy, with particular interest in the early pancreatic cancer detection, can be achieved with the help of OC treatments. To proceed with the study of pancreas tissues under OC treatments, it is necessary to evaluate its optical properties, especially its RI for a wide spectral range. Only after obtaining such data, the variations induced by OC treatments can be truly evaluated.

Regarding the evaluation of the RI of pancreas, only two studies have been published so far. One presents the RI of porcine pancreas for 632.8 nm at 20 ± 2 °C [41] and the other presents the calculated dispersion for human pancreas at 25 °C between 450 and 1550 nm [42].

In the present study, we measured the RI of rabbit pancreas tissues at wavelengths in the visible and NIR and calculated the corresponding dispersion for this

spectral range. The methodology used in this study is described in Section 2, and the obtained results and discussion are presented in Section 3.

2 Materials and methods

In order to measure the refractive index of the pancreas, at different wavelengths, and calculate its dispersion, the total internal reflection method was used [23, 24]. The sample preparation, experimental methodology and dispersion calculation are described in the following subsections.

2.1 Tissue samples

The pancreas of three recently sacrificed rabbits were dissected and frozen for 24 h. Fig. 1 shows one of those pancreas.

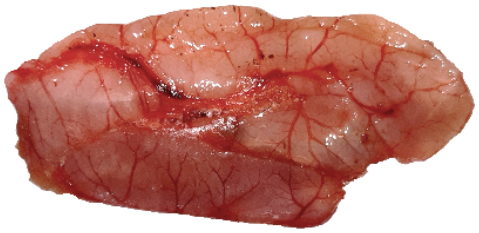

Fig. 1 One of the rabbit pancreas used in the RI measurements during thawing at room temperature.

One tissue sample with 1 cm × 1 cm × 3 mm was taken from each of the three rabbit pancreas, while they were still frozen. All the samples were prepared with a thickness of 3 mm and completely flat and uniform surfaces to perfectly adhere to the prism surface, without creating air bubbles in-between. These samples were kept in saline for 10 min and then were cleaned to remove outside remains of the solution.

2.2 Measurement procedure

Each sample was submitted to measurements with different lasers to obtain the pancreas RI at discrete wavelengths in the visible and NIR range.

The lasers used in this study had emission wavelengths at 401.4, 534.6, 626.6, 782.1, 820.8, and 850.7 nm. All these lasers are laser diodes from Edmund Optics, with the exception of the 534.6 nm and 626.6 nm lasers. The 534.6 nm laser is from Kvant (Slovakia) and the 626.6 nm laser is from Pasco (USA). The emitting power of all lasers was 5 mW or less and their emitting wavelengths were verified with a spectrometer from Avantes™.

For a particular set of measurements with a particular tissue sample and a particular laser, the tissue sample was placed in perfect contact with the base of the prism in the internal reflection setup (see Fig. 2).

A laser emitting at a particular wavelength entered the prism by another surface, where by refraction, was redirected to the prism/tissue interface. A reflected beam at this interface exited the prism through the third interface, where a detector (laser power sensor from Coherent with spectral range from 0.15 μm to 11 μm) connected to an electrical voltmeter (from Wavetek Meterman) was placed to collect the signal.

The prism was placed over a rotating stage (constructed in our lab – see Fig. 2), which allowed to vary the angle of incidence of the beam over the setup. As the incidence angle varied, the detector was also rotated to detect the reflected beam at each angular position.

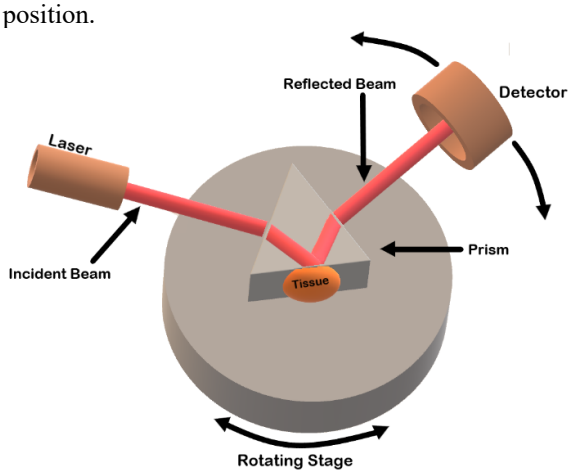

Fig. 2 Total internal reflection setup for RI measurements.

The dispersion prism used in these measurements is a SCHOTT N-SF11 prism acquired from Edmund Optics, with a wavelength dependence for its RI as presented in Fig. 3.

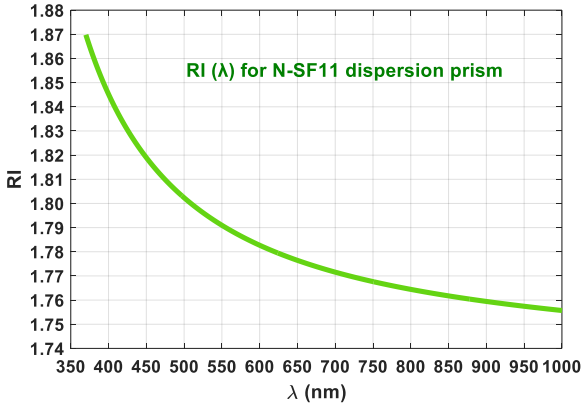

Fig. 3 Refractive index as a function of wavelength for the N-SF11 dispersion prism.

The curve presented in Fig. 3 is described by the Sellmeier equation [43], at 20 °C:

$$n^2 - 1 = \frac{K_1\lambda^2}{\lambda^2 - L_1} + \frac{K_2\lambda^2}{\lambda^2 - L_2} + \frac{K_3\lambda^2}{\lambda^2 - L_3}, \qquad (1)$$

where the Sellmeier coefficients have the following values for the SCHOTT N-SF11 glass: $K_1 = 1.7376$, $K_2 = 0.3137$, $K_3 = 1.8988$, $L_1 = 0.0132$, $L_2 = 0.0623$, and

$L_3 = 155.2363$. According to Ref. [43], since λ is represented in μm in Eq. (1), K_1, K_2 and K_3 are dimensionless coefficients, without units, while L_1, L_2 and L_3 are represented in μm^2.

Three sets of measurements were performed for each laser, one per tissue sample. In each individual study, temperature was kept constant at 20 °C, and the following measuring procedure was performed:

1. The sample was placed in perfect contact with the prism base (see Fig. 2).
2. Illumination of the setup was made with the laser beam through one side of the prism.
3. The reflected beam was collected with a photocell, connected to a voltmeter to read the electrical potential.
4. This measuring procedure was repeated for several incidence angles (α) between the incident laser beam and the normal to the air/prism interface. The angular resolution for these measurements was 1°.

Such procedure was repeated for the other lasers. The collected data from each set of measurements needed to be submitted to calculations to obtain the RI of pancreas at the wavelengths of the lasers used. The following sub-section describes these calculations.

2.3 RI calculations

Considering Fig. 2, and since the incident and reflected angles for the beam can only be measured outside the prism, at the prism/air interfaces, the Snell-Descartes equation needed to be used to convert the angle of the incident (or reflected) beam as measured outside the prism (α) to the incident (or reflected) angle at the prism/tissue interface (θ) [44]:

$$\theta = \beta - \arcsin\left[\frac{1}{n_{prism}} \times \sin(\alpha)\right], \tag{2}$$

with β representing the internal angle of the prism (60° in our case) and n_{prism} representing the RI of the prism at the wavelength of the laser in use (see Fig. 3).

Considering the electrical potential measurements and the corresponding angles at the prism/tissue interface, as obtained with Eq. (2), a reflectance curve was calculated as [25]:

$$R(\theta) = \frac{V(\theta) - V_{noise}}{V_{laser} - V_{noise}}, \tag{3}$$

with the potential measured at angle θ represented by $V(\theta)$, the potential measured with background light represented by V_{noise} and the potential measured directly from the laser represented by V_{laser}.

Once the reflectance curve was calculated with Eq. (3), the critical angle of reflection (θ_c) needed to be obtained from it. To identify such angle from the curve, its first derivative was first calculated. Such calculation was made according to [25]:

$$deriv(\theta) = \frac{R(\theta_i) - R(\theta_{i-1})}{\theta_i - \theta_{i-1}}, \tag{4}$$

where θ_i and θ_{i-1} are the consecutive angles of measurement and $R(\theta_i)$ and $R(\theta_{i-1})$ are the corresponding reflectance at those angles. As previously observed in other studies [23, 24], those derivatives will present a strong peak, whose central angle identifies the critical angle for each set of measurements.

By representing the curve for the first derivative, the value of θ_c was identified and then used in Eq. (5) to calculate the RI of the pancreas (n_{tissue}) at the laser wavelength [7]:

$$n_{tissue}(\lambda) = n_{prism}(\lambda) \times \sin(\theta_c). \tag{5}$$

Since three sets of measurements were performed with a particular laser, mean and standard deviation values for n_{tissue} provide higher accuracy and describe data dispersion between samples [7, 25].

Such calculation procedure was performed for each laser used in the RI measurements, so that the mean n_{tissue} values can be fitted with appropriate curves to obtain pancreas dispersion.

According to literature [2, 3, 7, 12, 18, 23–25, 27, 42], the most common dispersion equations to fit discrete RI data from biological tissues are the Cauchy (Eq. (6)), the Conrady (Eq. (7)) and the Cornu (Eq. (8)) equations [7, 25]:

$$n_{tissue}(\lambda) = A + \frac{B}{\lambda^2} + \frac{C}{\lambda^4}, \tag{6}$$

$$n_{tissue}(\lambda) = A + \frac{B}{\lambda} + \frac{C}{\lambda^{3.5}}, \tag{7}$$

$$n_{tissue}(\lambda) = A + \frac{B}{(\lambda - C)}, \tag{8}$$

where A, B and C are the Cauchy, Conrady, or Cornu parameters, that are obtained during the fitting of the experimental data.

All these curves were tested to fit the experimental RI data obtained for pancreas. Such data fittings were made using the Curve Fitting Tool (CFTOOL) of MATLAB™.

The results obtained and their discussion are presented next.

3 Results and discussion

After performing all experimental measurements, we started by calculating the reflectance curves for each set of measurements with each laser. Those reflectance curves, as calculated with Eq. (3), are presented in Fig. 4.

Using Eq. (4), we calculated the first derivative of the reflectance curves presented in Fig. 4 to obtain the values of θ_c. Those curves are presented in Fig. 5 for the measurements with each laser.

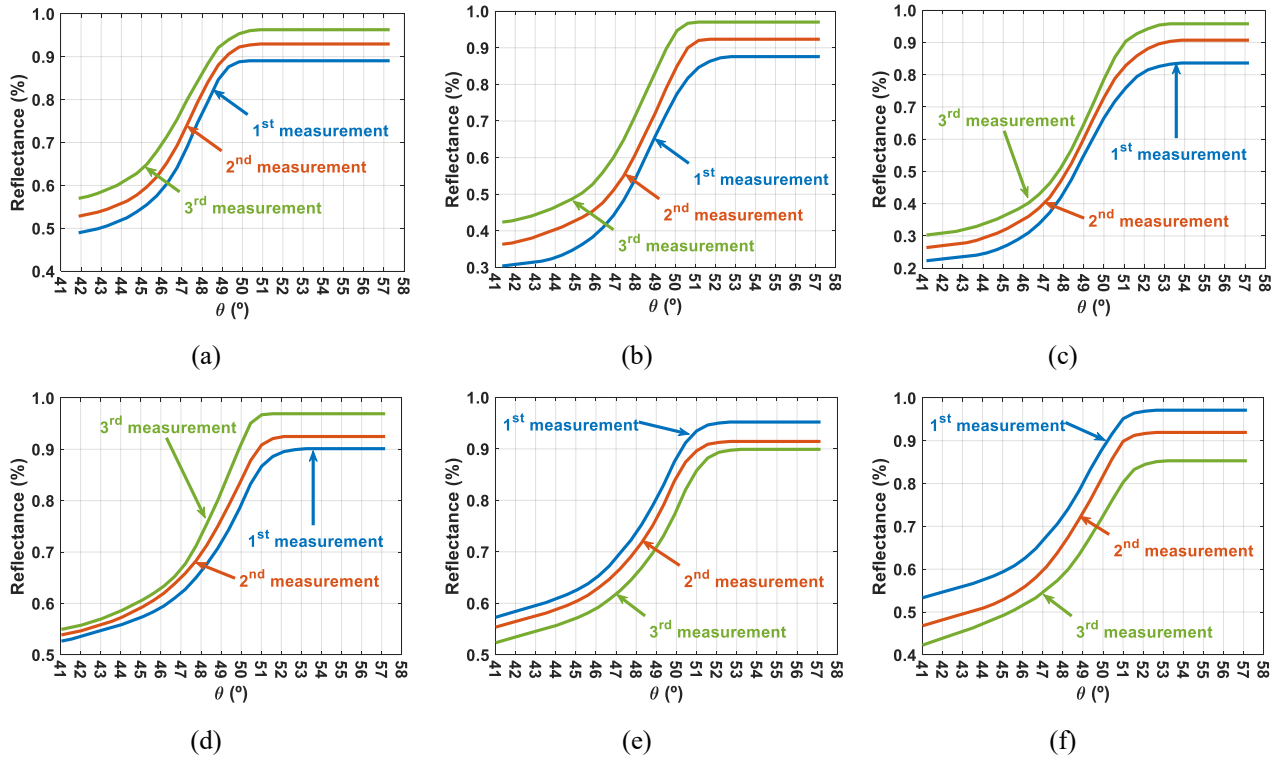

Fig. 4 Reflectance curves for the studies with the: 401.4 nm (a), 534.6 nm (b), 626.6 nm (c), 782.1 nm (d), 820.8 nm (e) and 850.7 nm (f) lasers.

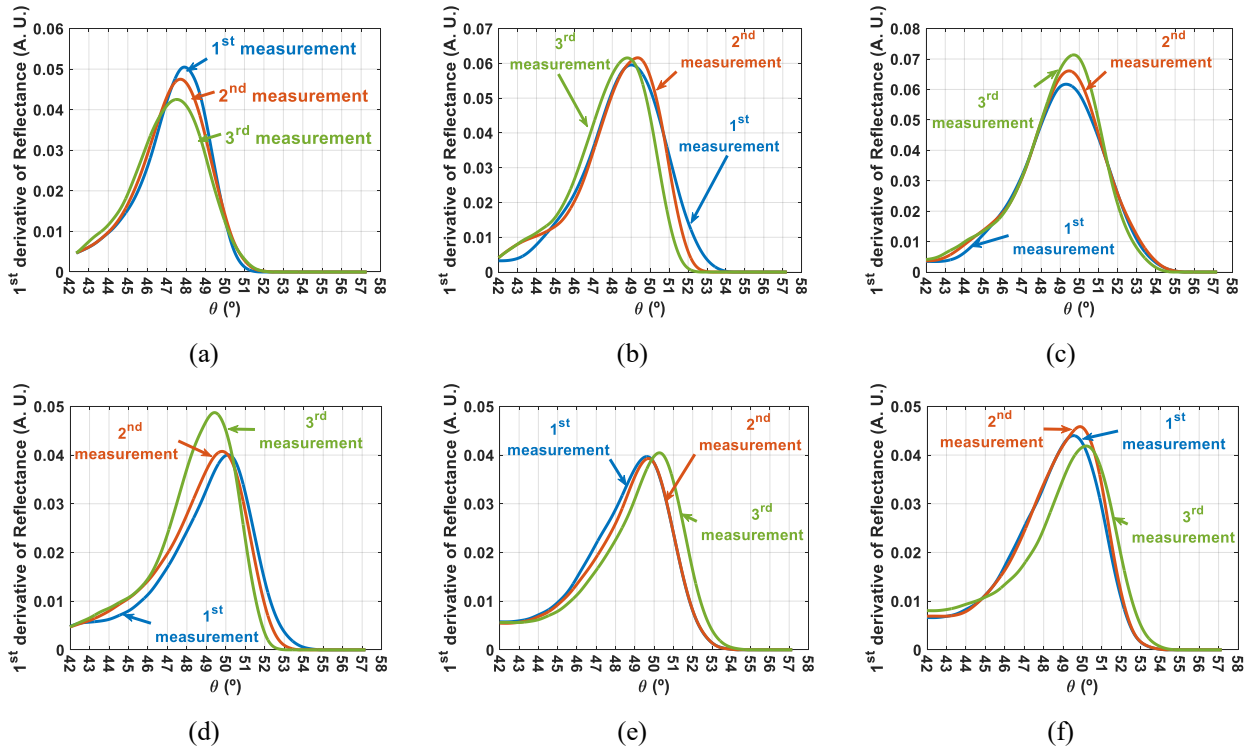

Fig. 5 First derivative of the reflectance curves for the studies with the: 401.4 nm (a), 534.6 nm (b), 626.6 nm (c), 782.1 nm (d), 820.8 nm (e) and 850.7 nm (f) lasers.

The values of θ_c as obtained from the graphs in Fig. 5 are presented in Table 1.

Using the θ_c values presented in Table 1 in Eq. (5), we calculated the corresponding n_{tissue} values. Those values, the mean and SD for each laser wavelength are presented in Table 2.

Using the CFTOOL in MATLAB, we fitted the mean RI values in Table 2 with the Eqs. (6), (7) and (8) for comparison. Fig. 6 presents such calculated dispersions for the spectral range of the experimental measurements (401–851 nm), along with some data for pancreas RI as collected from literature [41, 42].

Table 1 θ_c values obtained from the graphs in Fig. 5.

	θ_c (deg) per measurement		
Laser	**1st**	**2nd**	**3rd**
401.4 nm	47.9	47.7	47.5
534.6 nm	49.0	49.3	48.8
626.6 nm	49.3	49.5	49.7
782.1 nm	50.1	49.8	49.4
820.8 nm	49.6	49.7	50.3
850.7 nm	49.5	49.9	50.2

Table 2 Calculated n_{tissue} data for each laser wavelength.

	n_{tissue}				
λ (nm)	**1st**	**2nd**	**3rd**	**Mean**	**SD**
401.4	1.3688	1.3643	1.3604	1.3645	0.0042
534.6	1.3542	1.3612	1.3499	1.3551	0.0057
626.6	1.3491	1.3521	1.3572	1.3528	0.0041
782.1	1.3411	1.3489	1.3552	1.3484	0.0071
820.8	1.3429	1.3447	1.3560	1.3479	0.0071
850.7	1.3409	1.3474	1.3537	1.3473	0.0064

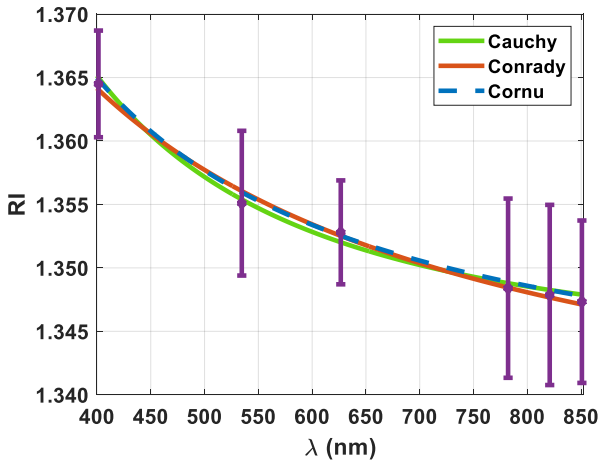

Fig. 6 Mean n_{tissue} data and calculated dispersions.

Fig. 6 shows that all curves provide good fitting of our experimental data for this range. All the calculated curves fall within the SD bars for each laser wavelength. Such SD bars present higher values for the longer wavelengths, already inside the NIR, a fact that is correlated with the visual difficulty in the alignment of invisible laser beams during measurements.

The calculated equations that describe the dispersions represented in Fig. 6 were the following:

$$n_{tissue}(\lambda) = 1.343 + \frac{3542}{\lambda^2} + \frac{0.1576}{\lambda^4} \quad \text{(Cauchy)}, \tag{9}$$

$$n_{tissue}(\lambda) = 1.332 + \frac{12.86}{\lambda} + \frac{0.1576}{\lambda^{3.5}} \quad \text{(Conrady)}, \tag{10}$$

$$n_{tissue}(\lambda) = 1.337 + \frac{7.915}{(\lambda - 117)} \quad \text{(Cornu)}. \tag{11}$$

The R-square values obtained in these fittings were: 0.994 (Cauchy and Conrady) and 0.997 (Cornu).

Comparing the data in these curves with data in literature, we see that the rabbit pancreas has a similar RI to the one from porcine pancreas at 633 nm – 1.3521 for rabbit (our study) and 1.3517 for porcine (Ref. [41]). Since the two results were obtained at 20 °C, their similarity makes perfect sense. Comparing our data with the human pancreas dispersion published in Ref. [42], which was calculated with only the first two terms in Eq. (6), our values within the visible–NIR range are higher, but we need to consider the difference in temperatures between studies.

As indicated in the introduction, the knowledge of tissue dispersion from the deep-UV to the infrared is highly important for a wide range of applications. Due to this interest, we extended the calculated dispersions to the spectral range between 200 and 1000 nm and looked in literature to find dispersions of tissues or tissue-like materials for comparison.

The only data for tissue or tissue-like dispersion that we could find for that spectral range, corresponds to histologic rat liver sections, which were initially fixed in Bouin's, Zenker's or Carnoy's fluid, then embedded and cut in paraffin and later deparaffinized in xylene [45]. Xylene is known as an OCA, and is also known to be toxic [46], meaning that the histologic preparation of those samples have altered the native dispersion of the liver sections. These changes are due to two processes. First, by embedding the liver samples in paraffin, a dehydration of the samples occurs, leading to an increase of the entire dispersion. Second, by deparaffinizing the samples in xylene leads to a RI matching mechanism, which further increases the sample's dispersion, in particular in the deep-UV, where the RI of proteins is bigger.

Although these changes occurred in the liver's dispersion, the contributions of collagen, DNA and hemoglobin to that dispersion remained unchanged, meaning that it is still the better approximation available in literature for the spectral range of interest. Retrieving that dispersion from Ref. [45], we modified its scale factor and baseline to match our experimental results for normally hydrated soft tissue (the complete rat liver

dispersion was multiplied by 0.34 and then we added 0.83 to it). By multiplying by 0.34, we reversed the dehydration and RI matching effects in a certain extent. Different values were tried in this rescaling process, but the ones indicated above were the ones that provided the best match to our experimental data.

To have a wide-band view, such rescaled dispersion and the calculated dispersions for the rabbit pancreas are presented in Fig. 7 for comparison.

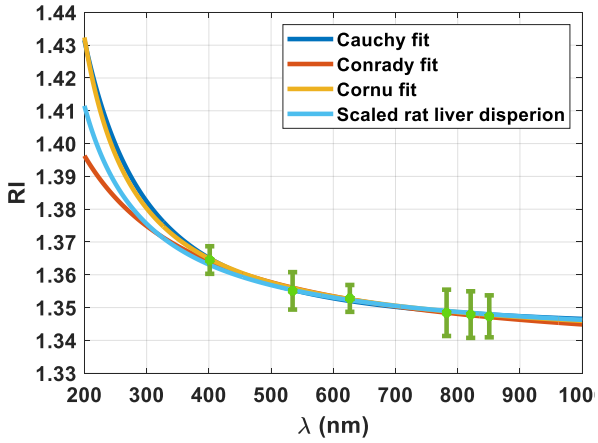

Fig. 7 Various dispersions for comparison.

Analyzing the various curves in Fig. 7, we see that the adjusted dispersion from rat histologic sections is also a good fit to our experimental data between 401 and 851 nm. It is also contained within the SD bars of our experimental data. For longer wavelengths, such adjusted dispersion is in better agreement with the Cauchy and Cornu dispersions, while in the deep-UV it falls almost in the middle of the calculated Conrady and the Cauchy/Cornu dispersions. Such positioning of the rescaled rat liver dispersion in-between the Conrady and the Cauchy/Cornu dispersions may be related to the RI matching of proteins, which was not completely reversed by our mathematical arrangement.

This means that, considering the UV-range, where major differences are observed, we cannot be sure which of the calculated dispersions for the pancreas is the more precise. They all may have equal probability to describe the pancreas dispersion in this range. To be sure, further studies are necessary. One possible approximation to get accurate dispersion for pancreas in the UV range is to obtain the spectrum of the absorption coefficient of pancreas and then through Kramers-Kronig (K-K) relations, calculate the real part of the RI [47].

Such procedure has been used in other studies [19, 47, 48], and in addition it provides more information, since spectral signatures of the pancreas can be seen in the dispersion after the calculation with the K–K relations. The calculated dispersions, as described by Eqs. (9), (10), and (11) do not show such spectral signatures due to the fact that they were obtained from measurements at discrete wavelengths. To obtain the pancreas dispersion between 200 and 1000 nm through K-K relations, the absorption coefficient spectrum ($\mu_a(\lambda)$) in that range must be obtained from spectral measurements. Then, the imaginary part of the RI ($\kappa(\lambda)$) of the pancreas can be calculated from $\mu_a(\lambda)$ [47]:

$$\kappa(\lambda)=\frac{\lambda}{4\pi}\mu_a(\lambda). \tag{12}$$

After calculating $\kappa(\lambda)$, the real part of pancreas RI ($n_{\text{tissue}}(\lambda)$) can be calculated through the following K-K relation [47,48]:

$$n_{tissue}(\lambda)=1+\frac{2}{\pi}\int_0^{\infty}\frac{\lambda}{\Lambda}\times\frac{\lambda}{\Lambda^2-\lambda^2}\kappa(\lambda)\,d\Lambda, \tag{13}$$

with Λ representing the integrating variable and λ representing a fixed wavelength that can be tuned for better vertical adjustment of the calculated dispersion to the one obtained from discrete data. In previous studies that we have made for other tissues [4, 13, 14, 19], we observed that by tuning λ, a better vertical alignment was obtained between the dispersion that results from calculations with Eqs. (12) and (13) and the dispersion that was calculated from discrete RI measurements.

This better adjustment is obtained if some dispersion, even for a shorter spectral range, such as the one obtained from discrete measurements through the total internal reflectance is available [4, 13].

Returning to the calculated dispersions for pancreas, as presented in Fig. 6 and described by Eqs. (9), (10), and (11), and considering only the wavelength range between 401 and 851, they all provide a good fit of our experimental data.

4 Conclusion

The RI values of rabbit pancreas were obtained from measurements acquired with the total internal reflection setup.

Three dispersion curves were calculated using the most common equations to fit discrete RI data from biological tissues: the Cauchy, the Conrady and the Cornu equations. All these curves fit the experimental data well in the visible-NIR range, but in the UV range, the curves calculated with the Cauchy and the Cornu equations present a faster decrease with wavelength than the one calculated with the Conrady equation. Such difference motivates further studies to inquire which of these curves provides an accurate fitting for the pancreas dispersion in the UV range.

For visible wavelengths, our data fits well with published data for porcine pancreas, although a single value for 633 nm is available in literature. A comparison with data in literature for human pancreas shows some significant differences, which are probably related to the difference in temperatures used in both studies.

After calculating the three dispersion curves that fit our data, it is our plan to continue this research with rabbit pancreas by perform spectral measurements to estimate the wavelength dependence of the optical properties of this tissue from the deep-UV to the NIR. In

those estimations, we will use the $\mu_a(\lambda)$ of the pancreas to calculate real dispersion through the K-K relations. We will use that dispersion to compare with the ones obtained in this study to check which one is the best. After such selection is made, we intend to use the selected pancreas dispersion in further studies that involve OC treatments.

Disclosures

All authors declare that there is no conflict of interests in this paper.

Acknowledgements

This research was supported by the Portuguese grant FCT-UIDB/04730/2020. VVT was supported by RFBR grant 18-52-16025.

References

1. Z. Wang, K. Tangella, A. Balla and G. Popescu, "Tissue refractive index as a marker of disease," Journal of Biomedical Optics 16(11), 116017 (2011).
2. P. Giannios, K. G. Toutouzas, M. Matiatou, K. Stasinos, M. M. Konstadoulakis, G. C. Zografos, and K. Moutzouris, "Visible to near-infrared refractive properties of freshly-excised human-liver tissues: marking hepatic malignancies," Scientific Reports 6, 27910 (2016).
3. P. Giannios, S. Koutsoumpos, K. G. Toutouzas, M. Matiatou, G. C. Zografos, and K. Moutzouris, "Complex refractive index of normal and malignant human colorectal tissue in the visible and near-infrared," Journal of Biophotonics 10(2), 303–310 (2017).
4. S. Carvalho, I. Carneiro, R. Henrique, V. Tuchin, and L. Oliveira, "Lipofuscin-type pigment as a marker of colorectal cancer," Electronics 9(11), 1805 (2020).
5. F. Carpignano, G. Rigamonti, G. Mazzani, and S. Merlo, "Low-coherence reflectometry for refractive index measurements of cells in micro-capillaries," Sensors 16(10), 1670 (2016).
6. Z. Turani, E. Fatemizadeh, Q. Xu, S. Daveluy, D. Mehregan, and M. R. N. Avanaki, "Refractive índex correction in optical coherence tomography images of multilayer tissues," Journal of Biomedical Optics 23(7), 070501 (2018).
7. E. N. Lazareva, L. Oliveira, I. Yu. Yanina, N. V. Chernomyrdin, G. R. Musina, D. K. Tuchina, A. N. Bashkatov, K. I. Zaytsev, and V. V. Tuchin, "Refractive index measurements of tissue and blood and OCAS in a wide spectral range" in Tissue optical clearing: new prospects in optical imaging, D. Zhu, E. Genina, and V. Tuchin (Eds), CRC Press, Boca Raton, USA, to be published.
8. A. R. Knuettel, M. Boehlau-Godau, "Spatially confined and temporally resolved refractive index and scattering evaluation in human skin performed with optical coherence tomography," Journal of Biomedical Optics 5(1), 83–92 (2000).
9. J.-C. Lai, Z.-H. Li, and A.-Z. He, "Influence of complex refractive index on diffuse reflection of biological tissues," Chinese Physics Letters 22(2), 332–334 (2005).
10. A. K. Dunn, Light scattering properties of cells, PhD dissertation, University of Texas at Austin, Texas, USA (1997).
11. L. M. Oliveira, K. I. Zaytsev, and V. V. Tuchin, "Improved biomedical imaging over a wide spectral range from UV to THz towards multimodality," Proceedings SPIE 11585, 1158503 (2020).
12. L. M. C. Oliveira, V. V. Tuchin, The Optical Clearing Method: A New Tool for Clinical Practice and Biomedical Engineering, Springer, Cham, Switzerland (2019). ISBN: 978-3-030-33055-2.
13. N. Gomes, V. V. Tuchin, and L. M. Oliveira, "UV-NIR efficiency of the refractive index matching mechanism on colorectal muscle during treatment with different glycerol osmolarities," Journal of Biomedical Photonics & Engineering 6(2), 020307 (2020).
14. N. Gomes, V. V. Tuchin, and L. M. Oliveira, "Refractive index matching efficiency in colorectal mucosa treated with glycerol," IEEE Journal of Selected Topics in Quantum Electronics 27(4), 7200808 (2021).
15. O. A. Smolyanskaya, N. V. Chernomyrdin, A. A. Konovko, K. I. Zaytsev, I. A. Ozheredov, O. P. Cherkasova, M. M. Nazarov, J.-P. Guillet, S. A. Kozlov, Yu. V. Kistnev, J.-L. Coutaz, P. Mounaix, V. L. Vaks, J.-H. Son, H. Cheon, V. P. Wallace, Yu. Feldman, I. Popov, A. N. Yaroslavsky, A. P. Shkurinov, and V. V. Tuchin, "Terahertz biophotonics as a tool for studies of dielectric and spectral properties of biological tissues and liquids," Progress in Quantum Electronics 62, 1–77 (2018).
16. K. I. Zaytsev, A. A. Gavdush, N. V. Chernomyrdin, and A. O. Yurchenko, "Highly accurate in vivo Terahertz spectroscopy of healthy skin: Variation of refractive index and absorption coefficient along the human body," IEEE Transactions on Terahertz Science and Technology 5(5), 817–827 (2015).
17. I. Carneiro, S. Carvalho, R. Henrique, L. Oliveira, and V. V. Tuchin, "Measuring optical properties of human liver between 400 1000 nm," Quantum Electronics 49(1), 13–19 (2019).
18. I. Yu. Yanina, E. N. Lazareva, and V. V. Tuchin, "Refractive index of adipose tissue and lipid droplet measured in wide spectral and temperature ranges," Applied Optics 57(17), 4839 (2018).

19. I. Carneiro, S. Carvalho, R. Henrique, L. Oliveira, and V. V. Tuchin, "Measurement of optical properties of normal and pathological human liver tissue from deep-UV to NIR," Proceedings SPIE 11363, 113630G (2020).
20. R. Khan, B. Gul, S. Khan, H. Nisar, and I. Ahmad, "Refractive index of biological tissues: Review, measurement techniques and applications," Photodiagnosis and Photodynamic Therapy 33, 102192 (2021).
21. H. Li, S. Xie, "Measurement method of the refractive index of biotissue by total internal reflection," Applied Optics 35, 1793–1975 (1996).
22. A. N. Bashkatov, K. V. Berezin, K. N. Dvoretskiy, M. L. Chernavina, E. A. Genina, V. D. Genin, V. I. Kochubey, E. N. Lazareva, A. B. Pravdin, M. E. Shvachkina, P. A. Timoshina, A. K. Tuchina, D. D. Yakovlev, D. A. Yakovlev, I. Yu. Yanina, O. S. Zhernovaya, and V. V. Tuchin, "Measurement of tissue optical properties in the context of tissue optical clearing," Journal of Biomedical Optics 23(9), 091416 (2018).
23. I. Carneiro, S. Carvalho, R. Henrique, L. Oliveira, and V. V. Tuchin "Water content and scatterers dispersion evaluation in colorectal tissues," Journal of Biomedical Photonics & Engineering 3(4), 040301 (2017).
24. S. Carvalho, N. Gueiral, E. Nogueira, R. Henrique, L. Oliveira, and V. V. Tuchin, "Wavelength dependence of the refractive index of human colorectal tissues: comparison between healthy mucosa and cancer," Journal of Biomedical Photonics & Engineering 2(4), 040307 (2016).
25. I. Carneiro, S. Carvalho, R. Henrique, L. Oliveira, and V. V. Tuchin, "Simple multimodal optical technique for evaluation of free/bound water and dispersion of human liver tissue," Journal of Biomedical Optics 22(12), 125002 (2017).
26. H. Ding, J. Q. Lu, K. M. Jacobs, and X.-H. Hu, "Determination of refractive indices of porcine skin tissues and intralipid at eight wavelengths between 325 and 1557 nm," Journal of Optical Society of America A 22(6), 1151–1157 (2005).
27. H. Ding, J. Q. Lu, W. A. Wooden P. J. Kragel, and X.-H. Hu, "Refractive indices of human skin tissue at eight wavelengths and estimated dispersion relations between 300 and 1600 nm," Physics in Medicine and Biology 51(6), 1479–1489 (2006).
28. J. Wang, Z. Deng, X. Wang, Q. Ye, W. Zhou, J. Mei, C. Zhang, and J. Tian, "Measurement of the refractive index of hemoglobin solutions for a continuous spectral region," Biomedical Optics Express 6(7), 2536–2541 (2015).
29. Z. Deng, J. Wang, Q. Ye, T. Sun, W.-Y. Zhou, J. Mei, C. Zhang, and J. Tian, "Determination of continuous complex refractive index dispersion of biotissue based on internal reflection," Journal of Biomedical Optics 21(1), 015003 (2016).
30. B. Lewis, J. Mao, "Development of the pancreas and related structures," in The Pancreas: An Integrated Textbook of Basic Science, Medicine and Surgery, 3rd Ed., H. G. Beger, A. L. Warshaw, R. H. Hruban, M. W. Brüchler, M. M. Lerch, J. P. Neoptolemos,T. Shimosegawa, and D. C. Whitcomb (Eds.), Wiley-Blackwell, Hoboken, New Jersey, USA (2018).
31. A. P. Klein, "Pancreatic cancer: a growing burden," The Lancet 4(12), 895–896 (2019).
32. S. Mohammed, G. van Buren 2nd, and W. E. Fisher, "Pancreatic cancer: advances in treatment," World Journal of Gastroenterology 20(28), 9354–9360 (2014).
33. D. P. Ryan, T. S. Hong, and N. Bardeesy, "Pancreatic adenocarcinoma," New England Journal of Medicine 371(11), 1039–1049 (2014).
34. K. Yamaguchi, T. Okusaka, K. Shimizu, J. Furuse, Y. Ito, K. Hanada, T. Shimosegawa, and K. Okazaki, "Clinical practice guidelines for pancreatic cancer 2016 from the pancreas society: A synopsis," Pancreas 46(5), 595–604 (2017).
35. I. D. Fleming, J. S. Cooper, D. E. Henson, R. V. P. Hutter. B. J. Kennedy, G. P. Murphy, B. O'Sullivan, L. H. Sobin, and J. W. Yarbro (Eds.), American Joint Committee for Cancer: Cancer Staging Manual, Whiting Press, Chicago, USA (1978).
36. J. H. Hwang, M. J. Cobb, M. B. Kimmey, and X. Li, "Optical coherence tomography imaging of the pancreas: a needle-based approach," Clinical Gastroenterology and Hepatology 3(7 Suppl 1), S49–S52 (2005).
37. S. Y. Lee, W. R. Lloyd, M. Chandra, R. H. Wilson, B. McKenna, D. Simeone, J. Scheiman, and M. A. Mycek, "Characterizing human pancreatic cancer using quantitative tissue optical spectroscopy," Biomedical Optics Express 4(12), 2828 (2013).
38. R. H. Wilson, M. Chandra, J. Scheiman, D. Simeone, B. McKenna, J. Purdy, and M.-A. Mycek, "Optical spectroscopy detects histological hallmarks of pancreatic cancer," Optics Express 17(20), 17502–17516 (2009).
39. P. A. Timoshina, A. B. Bucharskaya, D. A. Alexandrov, and V. V. Tuchin, "Study of blood microcirculation of pancreas in rats with alloxan diabetes by Laser Speckle Contrast Imaging," Journal of Biomedical Photonics & Engineering 3(1), 020301 (2017).
40. O. A. Smolyanskaya, E. N. Lazareva, S. S. Nalegaev, N. V. Petrov, K. I. Zaytsev, P. A. Timoshina, D. K. Tuchina, Ya. G. Toropova, O. V. Kornyushin, A. Yu. Babenko, J.-P. Guillet, and V. V. Tuchin, "Multimodal Optical Diagnostics of Glycated Biological Tissues," Biochemistry (Moscow) 84, 124–143 (2019).
41. J.-C. Lai, Y.-Y. Zhang, A.-H. Li, H.-J. Jiang, and A.-Z. He, "Complex refractive index measurement of biological tissues by attenuated total reflection ellipsometry," Applied Optics 49(16), 3235–3238 (2010).

42. M. Matiatou, P. Giannios, S. Koutsoumpos, K. G. Toutouzas, G. C. Zografos, and K. Moutzouris, "Data on the refractive index of freshly-excised human tissues in the visible and near-infrared spectral range," Results in Physics 22, 103833 (2021).
43. Refractive Index Database (accessed 7 February 2021) [https://refractiveindex.info/].
44. Q. W. Song, C.-Yu Ku, C. Zhang, R. B. Gross, R. R. Birge, and R. Michalak, "Modified critical angle method for measuring the refractive index of bio-optical materials and its application to bacteriorhodopsin," Journal of the Optical Society of America B 12(5), 797–803 (1995).
45. M. T. Jansen, "On the refractive index of histological tissue sections in visible and in ultraviolet light," Experimental Cell Research 15(1), 239–242 (1958).
46. N. Alwahaibi, S. Aljaradi, and H. Alazri, "Alternative to xylene as a clearing agent in histopathology," Journal Laboratory Physicians 10(2), 189–193 (2018).
47. O. Sydoruk, O. Zhernovaya, V. V. Tuchin, and A. Douplik, "Refractive index of solutions of human hemoglobin from the near-infrared to the ultraviolet range: Kramers-Kronig analysis," Journal of Biomedical Optics 17(11), 115002 (2012).
48. J. Gienger, H. Groβ, J. Neukammer, and M. Bär, "Determining the refractive index of human hemoglobin solutions by Kramers-Kronig relations with an improved absorption model," Applied Optics 55(31), 8951–8961 (2016).